



Ambiguities in target motion estimation for general SAR measurements

Title	Ambiguities in target motion estimation for general SAR measurements
Item Type	Article
Authors	Garren, David Alan
Citation	Garren, David Alan. "Ambiguities in target motion estimation for general SAR measurements." IET Radar, Sonar & Navigation 10.9 (2016): 1720-1728.
URI	https://hdl.handle.net/10945/61079
Publisher	Institution of Engineering and Technology (IET)
Date Issued	2016
Rights	This publication is a work of the U.S. Government as defined in Title 17, United States Code, Section 101. Copyright protection is not available for this work in the United States.
Download date	2026-04-14 05:13:53
Link to Item	https://hdl.handle.net/10945/61079

Downloaded from NPS Archive: Calhoun

Ambiguities in target motion estimation for general SAR measurements

ISSN 1751-8784
 Received on 19th January 2016
 Revised 6th April 2016
 Accepted on 9th April 2016
 E-First on 23rd September 2016
 doi: 10.1049/iet-rsn.2016.0024
 www.ietdl.org

David Alan Garren¹ ✉

¹Department of Electrical and Computer Engineering, Naval Postgraduate School, Monterey, CA 93943, USA

✉ E-mail: dagarren@nps.edu

Abstract: This study investigates the ability to invert synthetic aperture radar (SAR) measurement data in order to obtain unique estimates of the underlying motion parameters of targets within the imaged scene. In particular, this investigation reveals that ambiguities exist in estimating the kinematics parameters of surface targets for cases of general bistatic SAR collections. Specifically, the current study presents a detailed methodology for constructing any number of alternate target trajectories which yield the same set of SAR measurements as that corresponding to the true target motion. Additionally, the target trajectory ambiguities of the current investigation are shown to remain even if the radar system obtains bistatic range-rate or Doppler measurements. Unambiguous kinematics estimates can be obtained only through additional constraints, as with assumptions that a given surface target lies on the one-dimensional locus of a road. Thus, the ability to localise and estimate unambiguous target motion parameters relies on the energy intensity patterns of the transmission and reception beams of the radar system. Overall, the current analysis provides a simple, and yet powerful, exposition of the nature of target trajectory ambiguities in monostatic and bistatic SAR imagery.

1 Introduction

The collection of radar measurement data for synthetic aperture radar (SAR) image formation cannot be performed instantaneously but instead requires a non-zero time interval. Mobile targets can be moving during this period, thus introducing radar cross-range offsets of the resulting smeared signatures in the SAR imagery relative to the true target locations. This analysis seeks to characterise the conditions required to obtain accurate estimates of the location and the other motion parameters for a given target based only on its SAR signature smear. In particular, this paper investigates this ability to uniquely invert general SAR measurement data in order to generate accurate estimates of the underlying motion of the moving targets within the imaged scene. Herein, the term ‘moving target’ refers to a generic surface mobile object having motion relative to the background of stationary scattering centres including the degenerate case of a stationary target.

Many researchers have examined the smeared artefacts produced by moving targets in SAR imagery. The signatures for such moving targets can be smeared beyond recognition due to a mismatch in the image formation processing filters and the target motion. Various researchers have developed methods to focus moving target smears [1–22].

There have also been studies of other issues of moving target signatures in SAR. In particular, some researchers [1–4] have examined the general features of mover smears. Others [5–17] have investigated the detection and focusing of moving target signatures. Recent analyses [23–28] have studied SAR signature morphology for surface targets moving with arbitrary motion. Additional researchers [29–34] have developed methods for improving the detection of moving targets in SAR imagery.

A number of researchers have investigated potential ambiguities in estimating the target kinematics parameters corresponding to any given input signature smear. In particular, [35–39] have demonstrated the details of target motion ambiguities for monostatic collections in which the radar transmitter and receiver are co-located. Specifically, these studies examine the case of uniform linear motion for both the radar and target during the SAR collection interval. These research showed that different assumed target cases – in particular, one for a stationary target and one for a

moving target – can yield identical phase histories. An additional example demonstrates that a slow target which is moving in the down-range direction relative to the radar can yield the same set of range measurements along the synthetic aperture as a faster target that is moving with an oblique direction with regard to the radar's down-range.

The current paper formalises the existence of this target motion ambiguity and explores the general conditions under which it applies. Specifically, the current analysis reveals the existence of a fundamental ambiguity in attempting to use a given set of SAR measurement data in order to obtain an accurate estimate of the target location and other motion parameters. Furthermore, this investigation demonstrates that these ambiguities exist for all motion parameters including the mean target position, velocity, acceleration, and all higher-order moments. Thus, even the geo-location of the mover is known to lie only within the radar beam footprint. Furthermore, it is shown that this ambiguity exists for cases of non-linear motion of the target, the radar transmitter, and the radar receiver. In addition, the current work reveals that this ambiguity remains even for bistatic collections in which the radar transmitter and receiver are not co-located. Specifically, this analysis develops a detailed procedure for constructing alternative target trajectories and thus effectively yields a proof by contradiction in attempting to use a single set of SAR data to determine a unique set of underlying target motion parameters.

This ambiguity in estimating target motion lies at the radar measurement domain prior to the application of any image formation processing. Thus, the conclusions contained herein apply to both stripmap and spotlight SAR image formation. In addition, it applies for all types of SAR image formation methodologies [40–44] including the range migration algorithm, the chirp scaling algorithm, the polar format algorithm, and the back projection algorithm.

The target trajectory ambiguities described herein are of a continuous nature, so that it is possible to construct alternate target trajectories that are approximately equal to the true trajectory, and it is also possible to construct alternate target trajectories that are more radically different from the true target trajectory. These target trajectory ambiguities are distinct from the discrete and well-separated ambiguities that occur in the range–Doppler processing of pulsed waveforms in moving target indication (MTI) radar. In

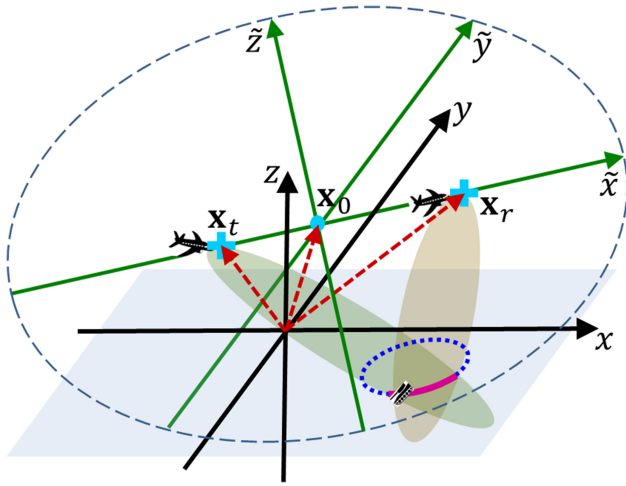


Fig. 1 3D ellipsoid corresponding to a given single bistatic radar range profile measurement, with the transmitter and receiver at the two foci and the 2D ellipse resulting from the intersection of this 3D ellipsoid with the ground plane. The region of overlap of the transmitter and receiver beam patterns intersects the solid arc of the 2D ellipse but not the dashed line of the remainder of the 2D ellipse

range–Doppler processing, the target range and radial velocity estimates are obtained to within integer constants of the unambiguous range and the unambiguous radial velocity, respectively. These range–Doppler ambiguities can be removed by transmitting waveform sets with different values of the pulse repetition frequency (PRF), assuming that the target motion is unmodified during these different waveform sets. In contrast, varying the time interval between transmission waveforms does not remove or even affect the target trajectory ambiguities investigated herein. Removal of some potential target motion hypotheses can only occur by either introducing additional constraints, e.g. target motion on a road, or by narrowing the spatial width of the transmission and/or reception beam patterns.

Section 2 describes the various assumptions regarding the radar return measurements along the synthetic aperture. Section 3 presents details of the true target motion and the resulting ambiguity surfaces. Section 4 develops a methodology for constructing alternate target trajectories that give the identical set of SAR measurements as that corresponding to the true target motion. Section 5 reveals that these target trajectory ambiguities remain even if the radar system obtains bistatic range-rate or Doppler measurements. Section 6 generates a specific numeric example in the construction of an alternate target trajectory. The conclusion is presented in Section 7.

2 Measurement assumptions

The assumptions regarding the radar measurement system and the unknown moving target are specified below:

- Each of the radar waveforms propagates at the constant speed-of-light c everywhere within the collection scene of interest.
- The radar transmitter and receiver are permitted to be: (a) co-located on the same platform, (b) located on different platforms, or (c) located at different positions on the same platform.
- Both the radar transmitter and the radar receiver are permitted to move with arbitrary trajectory and speed profiles in time, provided that the respective speeds, v_t and v_r , are non-relativistic such that $v_t \ll c$ and $v_r \ll c$, as is typical of radar collection systems.
- The trajectories of the radar transmitter and receiver are permitted to be known with arbitrary precision.
- An idealised point target is permitted to move with an arbitrary trajectory and speed profiles in time, provided that the target speed v_p is non-relativistic such that $v_p \ll c$, as is typical of radar collection systems.

- The target is constrained to move within the surface ground plane but is not constrained to lie on any particular road.
- The radar system collects an arbitrary number of bistatic range profile measurements along the full SAR collection interval.
- The bandwidth of each radar waveform is permitted to be arbitrarily large, so that the resulting range resolution and accuracy are permitted to be arbitrarily high as well.

In addition, the terminology ‘bistatic’ includes the degenerate ‘monostatic’ case in which the radar transmitter and receiver are co-located. This interpretation is used throughout the present analysis.

3 True target trajectory

The crux of this development hinges on the conclusion that different target trajectories can yield identical sets of radar measurements. That is, the relevant mapping is from *many* possible target trajectories to *one* resulting set of SAR measurements. Thus, if one is given a particular set of SAR measurements, then it is not possible to invert these data in order to obtain a unique target trajectory without the use of additional assumptions. The details of some of these additional constraints are outlined in [35] including the assumption that a given moving target lies on the one-dimensional (1D) locus of a road.

Begin with the assumed arbitrary trajectories of the radar transmitter, the receiver, and the target within 3D space. It is assumed that the trajectories of the transmitter and the receiver are known within some error, which is permitted to be arbitrarily small for these arguments. In addition, it is assumed that the trajectory of the surface target is unknown.

Assume that an arbitrary number N of waveforms is transmitted during the full synthetic aperture collection interval. Let $\tau_{t,n}$ be the mean value of the slow-time of the n th radar waveform that is emanated from the transmitter, and let $\tau_{r,n}$ be the mean time of its absorption in the receiver after scattering from the target. The temporal profile of this waveform is permitted to be arbitrarily narrow in terms of the fast-time t_f , corresponding to a Kronecker delta-function profile $\tilde{\delta}(t_f)$ in the limit of infinitely small width

$$\tilde{\delta}(t_f) \equiv \begin{cases} 1, & \text{if } t_f = 0 \\ 0, & \text{if } t_f \neq 0 \end{cases} \quad (1)$$

The size of the time interval between successive waveforms can vary in any manner. That is, this time interval is not required to be fixed for all pairs of successive waveforms. Define the time interval between the n th and $\{n+1\}$ th transmitted waveforms to be

$$\delta\tau_{t,n} \equiv \tau_{t,n+1} - \tau_{t,n}. \quad (2)$$

The next step is to compute the bistatic range measurement of a given idealised point target scattering centre. The measurement geometry for a single given waveform along the synthetic aperture is shown in Fig. 1. One ellipse focus corresponds to the 3D spatial location $\mathbf{x}_{t,n} = \{x_{t,n}, y_{t,n}, z_{t,n}\}$ of the transmission phase centre at the waveform emanation time $\tau_{t,n}$. The other focus corresponds to the location $\mathbf{x}_{r,n} = \{x_{r,n}, y_{r,n}, z_{r,n}\}$ of the receiver phase centre at the waveform absorption time $\tau_{r,n}$.

The transmitted waveform scatters from an idealised point target at location $\mathbf{x}_{s,n} = \{x_{s,n}, y_{s,n}, z_{s,n}\}$ at the time $\tau_{s,n}$. Assume a particular bandwidth Δf_n of waveform n . Since the waveform bandwidth is permitted to be arbitrarily large, this property is retained after scattering from a point target. That is, an impulse-like waveform profile is assumed to be retained after the scattering from the idealised point target scattering centre for the case of an arbitrarily large transmission bandwidth.

Thus, the radar system obtains a bistatic range measurement R_n of the target for the n th waveform. Define δR_n to be the error of this range measurement. The present development permits the transmitted waveform to have arbitrarily high bandwidth, so that

the corresponding error in the range measurement can be assumed to be arbitrarily small as well.

4 Alternate trajectory construction

The outline of this section begins with an idealised point scattering target with a given true motion profile within the ground plane during the synthetic aperture collection interval. The set of bistatic range profile measurements are generated corresponding to the true target motion. Next, a procedure is developed for constructing an alternative target scattering centre trajectory that gives the same set of range profile measurements. There is no constraint on the proximity of the alternate trajectory compared with that of the truth. That is, the alternate trajectory is not required to be infinitesimally close to the truth in terms of position, velocity, acceleration, or any higher-order motion parameter.

The development below applies for each transmitted waveform independently of all others. Thus, there is an implied index n corresponding to the particular waveform along the synthetic aperture. This index is suppressed until required in order to keep the notation less cumbersome.

Recall that the definition of a 3D ellipsoid implies that the sum $L \equiv \ell_t + \ell_r$ of the lengths ℓ_t and ℓ_r from a given point on the ellipsoid to the locations of the transmitter and receiver locations, respectively, is constant. Thus, the equation for the ellipsoid is determined entirely by the 3D locations of waveform transmission \mathbf{x}_t and waveform reception \mathbf{x}_r . The foci are placed at the locations of the radar transmitter \mathbf{x}_t at waveform emanation and the radar receiver \mathbf{x}_r at waveform absorption, as shown in Fig. 1. The origin of the ellipsoid is given by

$$\mathbf{x}_0 \equiv \frac{1}{2}\{\mathbf{x}_r + \mathbf{x}_t\}. \quad (3)$$

The focal length is equal to one-half of the magnitude of the distance between these two vectors

$$f \equiv \frac{1}{2}\|\mathbf{x}_r - \mathbf{x}_t\|. \quad (4)$$

Consider an arbitrary point $\mathbf{x} = \{x, y, z\}$ on the 3D ellipsoid within the overlap of the transmission and reception beam patterns. Define the lengths to this arbitrary point via

$$\ell_t \equiv \|\mathbf{x}_t - \mathbf{x}\|, \quad \ell_r \equiv \|\mathbf{x}_r - \mathbf{x}\|. \quad (5)$$

Then the bistatic range

$$R \equiv \frac{1}{2}\{\ell_t + \ell_r\} \quad (6)$$

defines the locus of possible sources for target scattering on the overlap of the transmission and reception beam patterns within the 3D ellipsoid. The factor of one-half is included so that R reduces to the standard range for monostatic SAR. These surfaces of constant range are spherical if the transmitter and receiver are co-located. If they are not co-located, then the surfaces of constant bistatic range are ellipsoidal, as a particular constant time-of-flight surface traces a 2D ellipse of revolution about the semi-major axis.

Define ellipsoid-centred coordinates $\{\tilde{x}, \tilde{y}, \tilde{z}\}$ so that the origin $\{0, 0, 0\}$ lies at the centre of the 3D ellipsoid, and the \tilde{x} -axis is aligned with the line connecting the two foci. The \tilde{y} and \tilde{z} coordinates are selected mutually orthogonal to the \tilde{x} -coordinate, wherein the \tilde{y} -coordinate lies in the horizontal direction relative to the ground plane. Since the transmitter and receiver locations lie at the foci, the spatial positions of these radar elements have the following forms:

$$\tilde{\mathbf{x}}_t = \{\tilde{x}_t, \tilde{y}_t, \tilde{z}_t\} = \{-f, 0, 0\}, \quad (7)$$

$$\tilde{\mathbf{x}}_r = \{\tilde{x}_r, \tilde{y}_r, \tilde{z}_r\} = \{f, 0, 0\}. \quad (8)$$

The definitions above imply the following form for the ellipsoid:

$$\frac{\tilde{x}^2}{a^2} + \frac{\tilde{y}^2}{b^2} + \frac{\tilde{z}^2}{b^2} = 1, \quad (9)$$

with a equal to the semi-major axis of the ellipsoid and b equal to the two semi-minor axes. The values of the two semi-minor axes are identical, since the loci of possible bistatic range measurements is given by a 2D ellipse of rotation about the axis joining the two foci.

Define $\Delta\tau$ equal to the round-trip fast-time of the waveform from the transmitter to the receiver

$$\Delta\tau \equiv \tau_r - \tau_t. \quad (10)$$

This fast-time difference is related to the bistatic range via

$$\Delta\tau = \frac{2R}{c}. \quad (11)$$

Consider the point on the ellipsoid along the semi-major axis which is closer to the receiver than the transmitter. The lengths to the transmitter and receiver are given by:

$$\ell_t = a + f, \quad \ell_r = a - f, \quad (12)$$

in terms of the definitions used in (9). Thus, (6) implies that the bistatic range is equal to the semi-major axis, i.e.

$$a = R = \frac{c\Delta\tau}{2}. \quad (13)$$

A point on the ellipsoid along a semi-minor axis is equal-distant from the transmitter and the receiver, so that $R = a = \ell_t = \ell_r$. Specifically, such a semi-minor axis point forms a triangle with the centre of the ellipsoid and one of the two foci, so that

$$\ell_t = \ell_r = \sqrt{f^2 + b^2} = a = R. \quad (14)$$

Thus, these equations determine the square of the semi-minor axis length

$$b^2 = R^2 - f^2 = \frac{\{c\Delta\tau\}^2 - \|\mathbf{x}_r - \mathbf{x}_t\|^2}{4}. \quad (15)$$

Equations (13) and (15) in (9) yield the following equation for the ellipsoid:

$$\frac{\tilde{x}^2}{\{c\Delta\tau\}^2} + \frac{\tilde{y}^2 + \tilde{z}^2}{\{c\Delta\tau\}^2 - \|\mathbf{x}_r - \mathbf{x}_t\|^2} = \frac{1}{4}. \quad (16)$$

Rotations and translations in 3D are required in order to place this ellipsoid with an arbitrary orientation and location relative to the ground plane to be imaged. To make these coordinate changes, it is necessary to define the relation between the natural ellipsoidal coordinates and the ground-plane coordinates of the formed SAR imagery. Define the vector along the semi-major ellipsoidal axis to be

$$\mathbf{w} \equiv \mathbf{x}_r - \mathbf{x}_t. \quad (17)$$

In addition, let $\{w_x, w_y, w_z\}$ denote the components of \mathbf{w} along the ground-plane unit vectors $\{\hat{\mathbf{x}}, \hat{\mathbf{y}}, \hat{\mathbf{z}}\}$. Then, define the elevation and azimuthal angles, respectively, of the 3D ellipsoid relative to the ground-plane coordinates via

$$-\frac{\pi}{2} \leq \Phi \equiv \arctan\left(\frac{w_z}{\sqrt{w_x^2 + w_y^2}}\right) \leq \frac{\pi}{2}, \quad (18)$$

$$-\pi < \Theta \equiv \arctan\left(\frac{w_y}{w_x}\right) \leq \pi. \quad (19)$$

In (19), the signs of w_x and w_y determine the quadrant of Θ , wherein a positive value of w_y implies that Θ lies between zero and π and a negative value gives an angle between $-\pi$ and zero.

The definition of the angles Θ and Φ enable the transformation from the ellipsoid-centred coordinates $\tilde{\mathbf{x}} = \{\tilde{x}, \tilde{y}, \tilde{z}\}$ to the ground-plane coordinates $\mathbf{x} = \{x, y, z\}$. To do so, first define an intermediate set of coordinates $\{x', y', z'\}$ via a rotation of Φ about the \tilde{y} -axis

$$x' = \tilde{x} \cos(\Phi) - \tilde{z} \sin(\Phi), \quad (20)$$

$$y' = \tilde{y}, \quad (21)$$

$$z' = \tilde{x} \sin(\Phi) + \tilde{z} \cos(\Phi). \quad (22)$$

The inverse transformation is given by

$$\tilde{x} = x' \cos(\Phi) + z' \sin(\Phi), \quad (23)$$

$$\tilde{y} = y', \quad (24)$$

$$\tilde{z} = -x' \sin(\Phi) + z' \cos(\Phi). \quad (25)$$

Next, transform from the intermediate coordinates $\{x', y', z'\}$ to the ground-plane coordinates via rotation of Θ about the z' -axis, followed by a translation to the ellipsoid centre:

$$x = x' \cos(\Theta) - y' \sin(\Theta) + X_0, \quad (26)$$

$$y = x' \sin(\Theta) + y' \cos(\Theta) + Y_0, \quad (27)$$

$$z = z' + Z_0. \quad (28)$$

In these equations, $\mathbf{x} = \{X_0, Y_0, Z_0\}$ is equal to the location of the centre of the 3D ellipsoid in terms of ground-plane coordinates $\{x, y, z\}$. The inverse transformation is given by

$$x' = \{x - X_0\} \cos(\Theta) + \{y - Y_0\} \sin(\Theta), \quad (29)$$

$$y' = -\{x - X_0\} \sin(\Theta) + \{y - Y_0\} \cos(\Theta), \quad (30)$$

$$z' = z - Z_0. \quad (31)$$

Inserting (23)–(25) and (29)–(31) into (16) yields the form of the 3D ellipsoid in terms of ground-plane coordinates $\{x, y, z\}$

$$\sum_{0 \leq \alpha + \beta + \gamma \leq 2} p_{\alpha\beta\gamma} x^\alpha y^\beta z^\gamma = 0, \quad (32)$$

wherein the $p_{\alpha\beta\gamma}$ are given by

$$p_{200} \equiv \rho, \quad (33)$$

$$p_{020} \equiv \omega, \quad (34)$$

$$p_{002} \equiv \gamma, \quad (35)$$

$$p_{110} \equiv \{\psi - \eta\} \sin(2\Theta), \quad (36)$$

$$p_{011} \equiv \{\xi - \eta\} \sin(\Theta) \sin(2\Phi), \quad (37)$$

$$p_{101} \equiv \{\xi - \eta\} \cos(\Theta) \sin(2\Phi), \quad (38)$$

$$p_{100} \equiv -2X_0\rho - Y_0\{\psi - \eta\} \sin(2\Theta) - Z_0\{\xi - \eta\} \cos(\Theta) \sin(2\Phi), \quad (39)$$

$$p_{010} \equiv -X_0\{\psi - \eta\} \sin(2\Theta) - 2Y_0\omega - Z_0\{\xi - \eta\} \sin(\Theta) \sin(2\Phi), \quad (40)$$

$$p_{001} \equiv -X_0\{\xi - \eta\} \cos(\Theta) \sin(2\Phi) - Y_0\{\xi - \eta\} \sin(\Theta) \sin(2\Phi) - 2Z_0\gamma, \quad (41)$$

$$p_{000} \equiv -\frac{1}{4} + X_0^2\rho + Y_0^2\omega + Z_0^2\gamma + X_0Y_0\{\psi - \eta\} \sin(2\Theta) + X_0Z_0\{\xi - \eta\} \cos(\Theta) \sin(2\Phi) + Y_0Z_0\{\xi - \eta\} \sin(\Theta) \sin(2\Phi). \quad (42)$$

Here, the parameters $\xi, \eta, \psi, \gamma, \rho$, and ω for a given waveform are defined by

$$\xi \equiv \{c\Delta\tau\}^{-2}, \quad (43)$$

$$\eta \equiv \{\{c\Delta\tau\}^2 - \|\mathbf{x}_r - \mathbf{x}_t\|^2\}^{-1}, \quad (44)$$

$$\psi \equiv \xi \cos^2(\Phi) + \eta \sin^2(\Phi), \quad (45)$$

$$\gamma \equiv \xi \sin^2(\Phi) + \eta \cos^2(\Phi), \quad (46)$$

$$\rho \equiv \psi \cos^2(\Theta) + \eta \sin^2(\Theta), \quad (47)$$

$$\omega \equiv \psi \sin^2(\Theta) + \eta \cos^2(\Theta). \quad (48)$$

4.1 Selection of first alternate trajectory position

The initial step is to select an alternate target location corresponding to the first bistatic range measurement. This spatial point corresponds to the initial target scattering location for an alternate target motion hypothesis. This alternate point is *not* constrained to lie with any particular distance or neighbourhood of the true target location for the initial measurement. However, this alternate point is constrained to lie on the 3D ellipsoid and within the overlap of the beam patterns of the transmitter and receiver.

Since the target scattering centre is also constrained to move on the ground plane, then the 3D ellipsoid is intersected with this plane in order to define a 2D ellipse of possible target scattering locations. Without loss in generality, select this ground plane to lie at $z = 0$. Then, (32) implies that this intersection of the 3D ellipse with the ground plane yields the following equations which must be solved in order to find the desired locus of alternate scattering points $\{x, y\}$:

$$\sum_{0 \leq \alpha + \beta \leq 2} p_{\alpha, \beta, 0} x^\alpha y^\beta = 0. \quad (49)$$

A graphic of this intersection of the 3D ellipsoid for a single waveform with the ground plane is shown in Fig. 1. The resulting 2D ground-plane ellipse is shown in this figure and in Fig. 2. Both figures present the region of overlap of the transmission and reception beam patterns as a solid arc of the 2D ground-plane ellipse, with the remainder of the ellipse as a dashed line.

Typically, the scattering location will lie somewhere within the overlap of the transmission and reception beam patterns corresponding to the bistatic range measurements. In rare instances, a highly reflective target can yield a sufficiently strong radar return within a beam pattern sidelobe of the transmitter or the receiver. If such cases are possible, then the solid section of the 2D ground-plane ellipse can be extended so as to encompass the main lobe and any relevant sidelobes. Under the general condition of an omnidirectional transmitter and an omnidirectional receiver, the beam patterns include the complete 2D ellipse, so that the entire ellipse can be considered in constructing alternate target trajectories.

In the trajectory construction methodology for the first waveform and all that follow, a specific process for generating alternate target locations must be developed. One such procedure

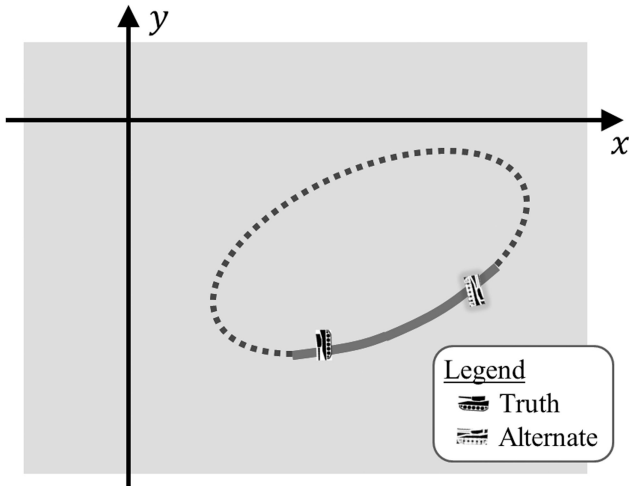


Fig. 2 2D ambiguity ellipse within the ground plane, corresponding to the bistatic range measurement for the initial waveform within the SAR collection interval

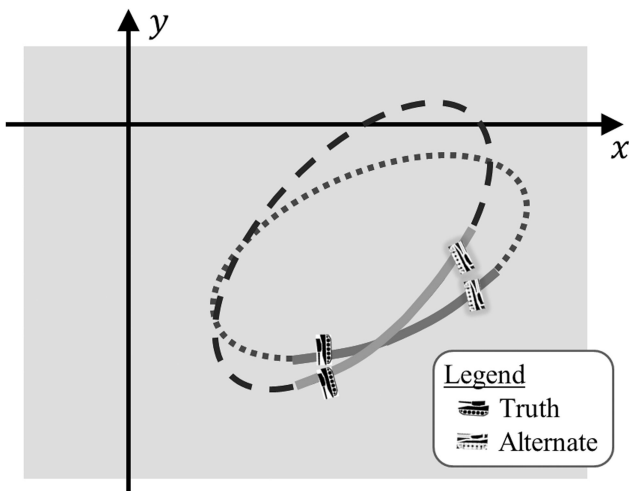


Fig. 3 Two ambiguity ellipses corresponding to two successive bistatic range measurements

begins with the selection of a value of x within the overlap of the transmission and reception beam patterns in the ground plane. It should be emphasised that the selected value of x need not lie near the true value for the actual target. Then, use the following quadratic equation that results from (49) to yield a closed-form solution for the value of y :

$$y = \frac{-p_{110}x - p_{010} \pm \sqrt{g(x)}}{2p_{020}}, \quad (50)$$

in terms of the function

$$g(x) \equiv \{p_{110}x + p_{010}\}^2 - 4p_{020}\{p_{200}x^2 + p_{100}x + p_{000}\}. \quad (51)$$

The value of x must be chosen so that $g(x)$ in (51) is non-negative in order to have real-valued solutions. In addition, the selection of x such that $g(x) > 0$ implies that there can be two solutions for y , which presents no issue since the goal is to construct any number of alternate target trajectories.

The scattering fast-time τ for any given instant in a target trajectory is determined by the parameters ℓ_t and ℓ_r of (5) via

$$\tau = \tau_t + \frac{\ell_t}{c}. \quad (52)$$

This equation applies for non-relativistic speeds of both the true target scattering event and any selected alternate target scattering

event. For a given alternate scattering event, the values of ℓ_t and ℓ_r are typically different from that of the true values due to waveform scattering from a hypothetical different target position on the relevant 2D ground-plane ellipse.

Note that a general bistatic radar system measures only the waveform travel time from the radar transmitter to the target and then to the radar receiver, which determines only the total waveform travel distance $\ell_t + \ell_r$. Therefore, this collection of radar echoes in bistatic radar systems does not directly yield ℓ_t , so that the exact fast-time τ of (52) corresponding to scattering off of the target is not directly measured. That is, the scattering fast-time τ is itself ambiguous but becomes specified when combined with a particular alternate target path in $\{x, y\}$ in the ground plane. For monostatic radar systems, the value of the scattering fast-time τ can be inferred directly to be the midpoint in time between that of radar transmission and reception.

In general, the discussion above demonstrates that the exact fast-time at which the radar scatters off of the target is not known for a general bistatic radar collection system. Nevertheless, the lack of this knowledge of the exact scattering fast-time does not prevent the ability to form a bistatic SAR image [43]. All of the usual Doppler measurements over a changing observation angle yield the small phase changes in the bistatic range measurements that are necessary in order to form an SAR image.

In summary, this methodology provides a prescription for constructing an alternate set of space and time values $\{x_1, y_1, 0, \tau_1\}_{\text{alt}}$ which gives the same bistatic range measurement for the first waveform as that obtained corresponding to the true target values $\{x_1, y_1, 0, \tau_1\}_{\text{true}}$. Earlier, the slow-time waveform index n was suppressed in order to prevent the notation from becoming too cumbersome but is now retained for clarity. The construction of alternate sets of space and time values for the successive waveform n values proceeds in a similar fashion.

4.2 Selection of second alternate trajectory position

Next, construct the 3D ellipsoid corresponding to the second waveform return. Again, the radar transmission and reception beam patterns are used to limit the possible target locations at the time of this scattering event. These possible points are determined by the sensor positions $\mathbf{x}_{t,2}, \mathbf{x}_{r,2}$, and the time-of-flight measurement $\Delta\tau_2$ corresponding to the second waveform. Specifically, select an alternate value of x that lies within the overlap of the transmission and reception beam patterns in the ground plane for this second bistatic range measurement. Then, use $\{x_{t,2}, x_{r,2}, \Delta\tau_2\}$ to generate values $\{\Phi_2, \zeta_2, \eta_2\}$ via (18), (43), and (44), which in turn yield the second set of alternate target spatial values $\{x_2, y_2, 0, \tau_2\}_{\text{alt}}$ via (50). The corresponding target scattering time is computed using (52).

Thus, this analysis has provided a process for constructing the first two sets of alternate space and time values via $\{x_1, y_1, 0, \tau_1\}_{\text{alt}}$ and $\{x_2, y_2, 0, \tau_2\}_{\text{alt}}$, corresponding to the first two bistatic range measurements. These concepts are illustrated using the two 2D ambiguity ellipses in Fig. 3. Recall that the time interval $\delta\tau_1$ of (2) between any two successive waveforms can be selected to be arbitrarily small.

However, kinematic constraints can limit the locus of possible locations of the target at the successive waveform returns. For example, speed constraints can limit the locations where the target can be located for the second radar return. Specifically, a target is limited by the distance that it can travel between successive waveform reflections according to its maximum possible speed.

Note that the location of the second target trajectory location effectively defines a mean speed over the interval between the first two waveform scattering events. In this selection process, there are two parameters that define the target motion in the ground plane during the time interval between these first two scattering events: (a) the mean target speed and (b) the mean target heading. Note that the selection of the second scattering event along a given alternate target trajectory is required to lie along the 1D locus of the relevant 2D ground-plane ellipse. This constraint effectively

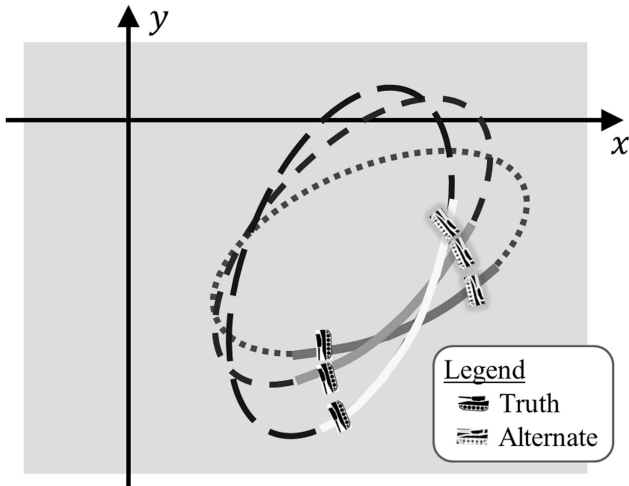


Fig. 4 Three ambiguity ellipses corresponding to three successive bistatic range measurements

reduces the number of degrees of freedom in the selection of the second scattering event from lying anywhere within the 2D ground plane to that of being restricted to be along the 1D locus of the section of the ground-plane ellipse lying in the intersection of the transmission and reception beam patterns. Correspondingly, there is only one degree of freedom in the selection of the alternate target 2D velocity within the ground plane, so that the selection of one component of the 2D velocity limits the possible values for the other.

4.3 Selection of third alternate trajectory position

Next, construct a 3D ellipse corresponding to the third waveform return. Again, select a value of x_3 within the overlap of the transmission and reception beam patterns for the third waveform, which need not lie near the true value. Then, use (50) to solve for a value of y_3 , giving an alternate target location at the third scattering event. The corresponding scattering time τ_3 is computed using (52). Thus, this procedure yields a construction of the first three sets of alternate space and time values via $\{x_1, y_1, 0, \tau_1\}_{alt}$, $\{x_2, y_2, 0, \tau_2\}_{alt}$ and $\{x_3, y_3, 0, \tau_3\}_{alt}$ which are consistent with the first three bistatic range measurements. Fig. 4 presents the 2D ambiguity ellipses corresponding to these first three radar returns.

Kinematic constraints limit the locus of possible locations of the point target at the third waveform return. For example, finite inertia constraint assumptions can limit the locations, where the target can be located for the third echo return. Specifically, there are additional constraints on a target's ability to accelerate based on engine power, or on a target's ability to decelerate in a braking manoeuvre. Finally, there can be constraints on a target's ability to change direction, based on of the friction between the tyres and the pavement.

As revealed above, there is one degree of freedom in the selection of the initial position in the ground plane for the first bistatic range measurement corresponding to the alternate target trajectory. In addition, there is one degree of freedom in the alternate target velocity within the ground plane for the second radar waveform. Similarly, for the third bistatic range measurement, there is one degree of freedom in selecting the 2D acceleration within the ground plane. Specifically, the selection of the third scattering event along a given alternate target trajectory is required to lie along the 1D locus of the relevant 2D ground-plane ellipse. This constraint effectively reduces the number of degrees of freedom in the selection of the third scattering event from lying anywhere within the 2D ground plane to that of being restricted to be along the 1D locus of the section of the ground-plane ellipse lying in the intersection of the transmission and reception beam patterns. Thus, though two degrees of freedom exist, in general, in the selection of the 2D acceleration of the alternate surface target within the ground plane, there is only one degree of freedom that is available in selecting the alternate target trajectory.

4.4 Selection of higher-order trajectory positions

At this point in the analysis, it is possible to define a general methodology for constructing alternate target trajectories through arbitrary order in the motion parameters. In general, use $\{x_{t,n}, x_{r,n}, \Delta\tau_n\}$ for the n th waveform in order to generate values $\{\Phi_n, \xi_n, \eta_n\}$ via (18), (43), and (44). These values, in turn, yield the alternate target position and time of $\{x_n, y_n, 0, \tau_n\}$ for the n th waveform via (50) and (52). In this fashion, the higher-order motion parameters for the alternate target trajectory can be constructed.

5 Range-rate or Doppler measurements

For the next stage of the analysis, the effects of Doppler modulation arising from the use of multiple bistatic target range measurements over slow-time are examined. Specifically, consider any two successive bistatic radar range measurements in the overall SAR collection. Assume that any one of the possible alternate target trajectories is selected consistent with the equations of Section 4. Specifically, the two alternate target positions corresponding to these two successive waveform scattering events are selected to lie on the two respective ground-plane ellipses. Thus, the two successive bistatic range measurements corresponding to this selected fictitious alternate target trajectory are identical with that obtained from the true target trajectory.

Next, the two successive bistatic range measurements can be used to estimate the instantaneous range-rate of the target, which is commonly referred to as the target 'Doppler'. First, recall that (2) gives the time interval $\delta\tau_{t,n}$ between these two successive bistatic range measurements indexed by n and $\{n+1\}$. Thus, the instantaneous target range-rate between the successive waveforms indexed by n and $\{n+1\}$ can be approximated by

$$R_n^{(1)} \cong \frac{R_{n+1} - R_n}{\delta\tau_{t,n}}. \quad (53)$$

Note that the range-rate estimates for both the true target trajectory and the selected fictitious alternate target trajectory are identical, since the corresponding bistatic range measurements R_{n+1} and R_n also are identical. Therefore, the estimation of the target range-rate $R_n^{(1)}$ does not offer any additional information to remove the fundamental target trajectory ambiguity that is the subject of the current analysis.

Also note that the analysis above applies in the limit in which the interval $\delta\tau_{t,n}$ between successive waveforms approaches zero, i.e.

$$R_n^{(1)} \equiv \lim_{\delta\tau_{t,n} \rightarrow 0} \frac{R_{n+1} - R_n}{\delta\tau_{t,n}}. \quad (54)$$

This result applies since the corresponding surfaces of constant bistatic range R converge to be overlapping as well, so that the range-rate definition is well defined. For this reason, it is assumed that there is no limit on the size of this time interval between successive waveforms.

These arguments can be extended to apply for successive estimates of a higher derivative range measurements, wherein the first range derivative is that corresponding to the target range-rate or Doppler measurements discussed above. For example, two successive range-rate estimates can be used to construct the target bistatic range acceleration estimate. This type of expression can be defined through arbitrary m th order via

$$R_n^{(m)} \equiv \lim_{\delta\tau_{t,n} \rightarrow 0} \frac{R_{n+1}^{(m)} - R_n^{(m)}}{\delta\tau_{t,n}}. \quad (55)$$

However, the corresponding bistatic range measurements of any derivative order are identical for the true target trajectory and any alternate fictitious trajectory selected according to the analysis of Section 4. Therefore, the fundamental target trajectory ambiguities

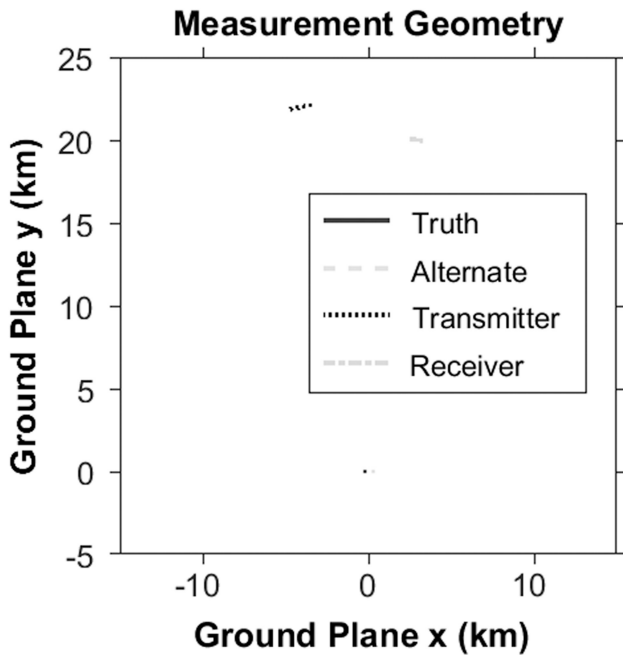


Fig. 5 Simulation geometry for the SAR measurements in this example, showing the trajectories of the radar transmitter and receiver. The trajectories of the true and alternate targets resolve to only approximate points near $\{x, y\} = \{0, 0\}$ at this scale

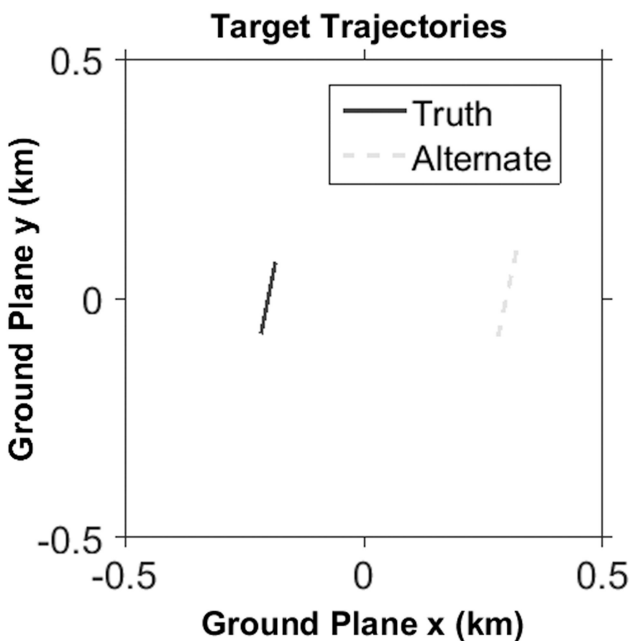


Fig. 6 Comparison of the trajectories of the true and alternate targets as shown by a zoomed image of Fig. 5

remain despite the fact that (55) can be used to yield estimates of higher-order kinematics quantities.

6 Alternate target trajectory example

In this section, a specific numeric example of an alternate target trajectory is generated in order to demonstrate the efficacy of the approach developed above. For this example, constant velocity motion is selected for both the radar transmitter and receiver. Certainly, the methodology developed herein is applicable for more general radar trajectories but the selection of constant velocities facilitates an understanding of the results. In addition, the true target is moving with a constant velocity during the SAR collection interval.

In the selected example, the PRF is selected to be 1 kHz, with 10,001 waveforms transmitted over a 10 s synthetic aperture time.

The mean positions of the radar transmitter, the radar receiver, and the moving target are selected to be $\{-4, 22, 1.2\}$, $\{3, 20, 1\}$, and $\{-0.2, 0, 0\}$ km, respectively, in terms of the ground-plane coordinates $\{x, y, z\}$ in units of metres. The corresponding values of the constant velocity vectors in terms of the same ground-plane coordinates are $\{150, 30, 0\}$, $\{100, -15, 0\}$, and $\{-3, -15, 0\}$ m/s, respectively, in units of metres per second.

Note that the values of $p_{\alpha, \beta, \gamma}$ are determined entirely by the trajectories of the radar transmitter and the radar receiver. Thus, these coefficients are vector functions of the slow-time waveform index n . Therefore, it is necessary to compute $g(x)$ in (51) for the entire slow-time interval of the SAR collection in order to ensure that the selected x values selected over the slow-time index n can give a valid alternate target trajectory for the entire SAR collection interval.

The generation of an alternate trajectory can be obtained by selecting a set of x points for each of the waveforms along the aperture. One possible prescription for selecting an alternate set of x points is to scale and shift the corresponding values for the true target trajectory. In this example, the extent of the x points was stretched by a factor of 1.3, followed by a shift of 0.5 km. Then, these values of x are used to compute the corresponding y values via (50), thus determining the alternate target locations $\{x, y, 0\}$ for each waveform along the synthetic aperture.

Fig. 5 presents the simulation geometry for the SAR measurements in this example, showing the trajectories of the radar transmitter and receiver. The trajectories of the true and alternate targets resolve to only approximate points near $\{x, y\} = \{0, 0\}$ at this scale. Fig. 6 shows the region of Fig. 5 near the origin, revealing that the alternate target traverses a distance that is a factor of ~ 1.3 greater than that of the true target trajectory. In addition, the mean orientation of the trajectories of the true and alternate targets is approximately identical.

Fig. 7 gives a plot of the speed variation of the alternate target trajectory over the entire synthetic aperture. Since this speed variation is < 0.2 m/s over the entire 10 s SAR collection interval, there would be little or no stress on brakes and engine. Similarly, Fig. 8 reveals that the heading of the alternate target trajectory varies by only 0.1° over the full collection interval, so that there would be little or no stress on tyres for this particular example.

Fig. 9 compares the temporal profiles of the bistatic range of the true and alternate target trajectories. This figure reveals that the values of the bistatic range over the full synthetic aperture collection interval are identical for the true and alternate target trajectories. Differences are on the order of $30 \mu\text{m}$ or less, which is due to machine numerical error.

7 Conclusion

This paper examines the ambiguities that exist in estimating the kinematics parameters of moving targets collected in general SAR measurements. In particular, it is shown that ambiguities exist in the estimated motion parameters of surface targets for cases of general bistatic SAR collections. Unambiguous kinematics estimates can be obtained only through additional constraints, as with assumptions that a given surface target lies on the 1D locus of a road. This investigation shows that all target motion parameters are ambiguous for any interval during the SAR collection including the target position, velocity, acceleration, and higher-order motion parameters. Thus, the ability to localise and estimate unambiguous target motion parameters relies on the energy intensity patterns of the transmission and reception beams of the radar system. An example was presented revealing that an ambiguous trajectory can be separated from the true target location by relatively large distance of 0.5 km.

This analysis has no limitations regarding the bandwidth of the transmission waveform. In effect, the waveform can be arbitrarily sharp in time via an infinitely narrow delta-function impulse. In addition, there is no limitation on the time interval between two successive waveforms. This time interval can be arbitrarily small, so that radar range measurements can follow a given scattering centre effectively in a continuous manner as the target moves during the synthetic aperture collection interval. Finally, the target

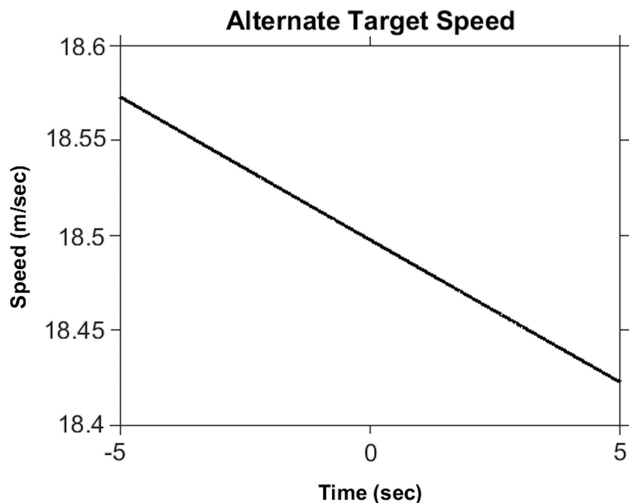


Fig. 7 Speed of the alternate target trajectory varies by only about 1% over the duration of the synthetic aperture

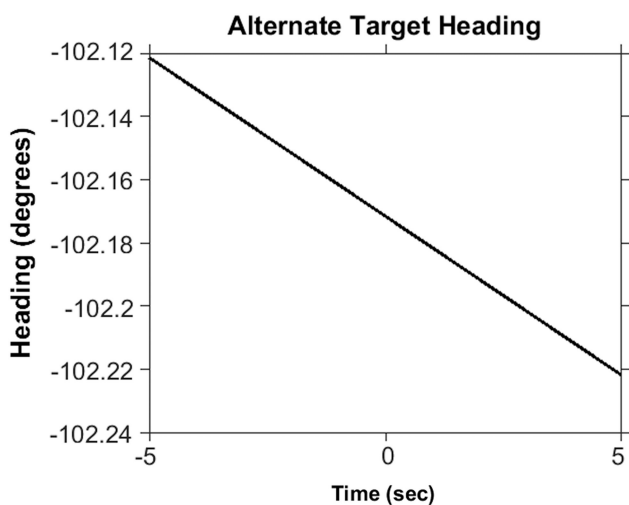


Fig. 8 Heading of the alternate target trajectory varies by only about 0.1° over the duration of the synthetic aperture

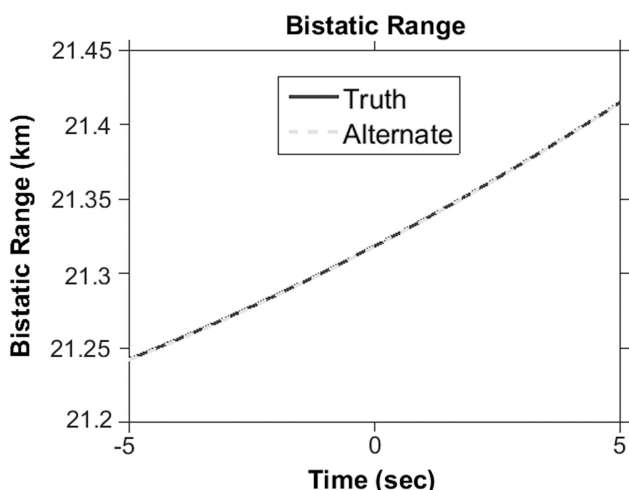


Fig. 9 Temporal profiles of the bistatic range over the full synthetic aperture collection interval are identical for the true and alternate target trajectories

can be an infinitely sharp point scattering centre, as is modelled in this analysis.

The target trajectory ambiguities investigated in this paper are of a continuous nature, and therefore distinct from the discrete ambiguities that occur in MTI range–Doppler processing. The range–Doppler ambiguity can be removed by transmitting

waveform sets with different PRFs but has no effect on the target trajectory ambiguities. Removal of the subject target trajectory ambiguities can only occur via additional constraints, e.g. target motion on a road, or by narrowing the transmission or reception beam patterns.

The subject target trajectory ambiguities are shown to exist for all motion parameters that can be used to describe a moving target including its mean position, velocity, acceleration, and all higher-order moments. Thus, even the geo-location of the mover is known to lie only within the radar beam footprint. In addition, relativistic corrections are expected to be minute, since typical speeds of both radars and targets are many orders of magnitude less than the speed of light. Therefore, the current paper presents a simple and powerful exposition of the nature of moving target trajectory ambiguities and a specific methodology for constructing alternate surface target trajectories for general SAR measurement systems.

8 Acknowledgments

DoD distribution statement A: Unlimited distribution. The author thanks AFRL for partial support of this work. The author thanks the anonymous reviewers in providing valuable suggestions to improve the quality of this paper. The views expressed in this document are those of the author and do not reflect the official policy or position of the Department of Defense or the U.S. Government.

9 References

- [1] Raney, R.K.: ‘Synthetic aperture imaging radar and moving targets’, *IEEE Trans. Aerosp. Electron. Syst.*, 1971, 7, pp. 499–505
- [2] Perry, R.P., DiPietro, R.C., Fante, R.L.: ‘SAR imaging of moving targets’, *IEEE Trans. Aerosp. Electron. Syst.*, 1999, 35, pp. 188–200
- [3] Fienup, J.R.: ‘Detecting moving targets in SAR imagery by focusing’, *IEEE Trans. Aerosp. Electron. Syst.*, 2001, 37, pp. 794–809
- [4] Cristallini, D., Pastina, D., Colone, F., *et al.*: ‘Efficient detection and imaging of moving targets in SAR images based on chirp scaling’, *IEEE Trans. Geosci. Remote Sens.*, 2013, 51, pp. 2403–2416
- [5] Jakowatz, C.V.Jr., Wahl, D.E., Eichel, P.H.: ‘Refocus of constant velocity moving targets in synthetic aperture radar imagery’. Proc. SPIE: Algorithms for Synthetic Aperture Radar Imagery V, April 1998, vol. 3370, pp. 85–95
- [6] Rigling, B.D.: ‘Image-quality focusing of rotating SAR targets’, *IEEE Geosci. Remote Sens. Lett.*, 2008, 5, pp. 750–754
- [7] Vu, V.T.S., Pettersson, T.K., Gustavsson, M.L., *et al.*: ‘Detection of moving targets by focusing in UWB SAR – theory and experimental results’, *IEEE Trans. Geosci. Remote Sens.*, 2010, 48, (10), p. 3799
- [8] Stojanovic, I., Karl, W.C.: ‘Imaging of moving targets with multi-static SAR using an overcomplete dictionary’, *IEEE J. Sel. Top. Signal Process.*, 2010, 4, pp. 164–176
- [9] Leducq, P., Ferro-Famil, L., Pottier, E.: ‘Matching-pursuit-based analysis of moving objects in polarimetric SAR images’, *IEEE Geosci. Remote Sens. Lett.*, 2008, 5, pp. 123–127
- [10] Fasih, A.R., Ertin, E., Ash, J.N., *et al.*: ‘SAR focusing performance for moving objects with random motion components’. Forty-second Asilomar Conf. on Signals, Systems and Computers, 2008. ACSSC 08, October 2008, pp. 1628–1632
- [11] Zhu, S., Liao, G., Qu, Y., *et al.*: ‘Ground moving targets imaging algorithm for synthetic aperture radar’, *IEEE Trans. Geosci. Remote Sens.*, 2011, 49, pp. 462–477
- [12] Cheney, M., Borden, B.: ‘Waveform-diverse moving-target spotlight SAR’. Proc. of the 2010 Int. Waveform Diversity and Design Conf., Niagara Falls, Canada, 8–13 August 2010, pp. 33–34
- [13] Xu, J., Zuo, Y., Xia, B., *et al.*: ‘Ground moving target signal analysis in complex image domain for multichannel SAR’, *IEEE Trans. Geosci. Remote Sens.*, 2012, 50, pp. 538–552
- [14] Yake, L., Yanfei, W., Chang, L.: ‘Detect and autofocus the moving target by its range walk in the time domain’ Proc. 2011 Int. Conf. Wirel. Commun. Signal Process., (WCSP), Nanjing, China, 9–11 November, 2011, pp. 1–5
- [15] Li, X., Deng, B., Qin, Y., *et al.*: ‘The influence of target micromotion on SAR and GMTI’, *IEEE Trans. Geosci. Remote Sens.*, 2011, 49, pp. 2738–2751
- [16] Deng, B., Qin, Y., Wang, H., *et al.*: ‘An efficient mathematical description of range models for high-order-motion targets in synthetic aperture radar’. Proc. of the 2012 IEEE Radar Conf., Atlanta, GA, 7–11 May 2012, pp. 6–10
- [17] DiPietro, R.C., Fante, R.L., Perry, R.P.: ‘Space-based bistatic GMTI using low resolution SAR’. IEEE Aerospace Conf. 1997, February 1997, vol. 2, pp. 181–193
- [18] Jao, J.K.: ‘Theory of synthetic aperture radar imaging of a moving target’, *IEEE Trans. Geosci. Remote Sens.*, 2001, 39, pp. 1984–1992
- [19] Garren, D.A.: ‘Method and system for developing and using an image reconstruction algorithm for detecting and imaging moving targets’. U.S. Patent 7456780 B1, November 2008
- [20] Mao, X.Z., Zhu, Z.-D.D.-Y.: ‘Signatures of moving target in polar format spotlight SAR image’, *Prog. Electromagn. Res.*, 2009, 92, pp. 47–64

- [21] Mao, X., Zhu, D., Wang, L., *et al.*: 'Response of polar format algorithm to moving target with consideration of wavefront curvature'. 2009 IEEE Radar Conf., Pasadena, CA, 2009
- [22] Linnehan, R., Perlovsky, L., Mutz, C., *et al.*: 'Detecting slow moving targets in SAR images'. Proc. of SPIE 5410, Radar Sensor Technology VIII and Passive Millimeter-Wave Imaging Technology VII, 12 August 2004, vol. 64
- [23] Garren, D.A.: 'Smear signature morphology of surface targets with arbitrary motion in spotlight synthetic aperture radar imagery', *IET Radar Sonar Navig.*, 2014, 8, pp. 435–448
- [24] Garren, D.A.: 'Signatures of braking surface targets in spotlight synthetic aperture radar'. Proc. of 2014 Sensor Signal Processing for Defence, Edinburgh, UK, 08–09 September 2014, pp. 51–55
- [25] Garren, D.A.: 'Signature predictions of surface targets undergoing turning maneuvers in spotlight synthetic aperture radar imagery'. Proc. of SPIE, Algorithms for Synthetic Aperture Radar Imagery XXII, Baltimore, MD, USA, 20–24 April 2015, pp. 4997–5008, vol. 9475, p. 94750A
- [26] Garren, D.A.: 'Signatures of surface targets with increasing speed in spotlight synthetic aperture radar'. 2015 IEEE Int. Radar Conf., Arlington, VA, USA, 11–15 May 2015, pp. 1114–1118
- [27] Garren, D.A.: 'Theory of two-dimensional signature morphology for arbitrarily moving surface targets in squinted spotlight synthetic aperture radar', *IEEE Trans. Geosci. Remote Sens.*, 2015, 53, pp. 4997–5008, Date of Publication to IEEE Xplore as an Early Access Article: 17 April 2015
- [28] Garren, D.A.: 'Signature morphology effects of squint angle for arbitrarily moving surface targets in spotlight synthetic aperture radar', *IEEE Trans. Geosci. Remote Sens.*, 2015, 53, pp. 6241–6251, Date of Publication to IEEE Xplore as an Early Access Article: 29 June 2015
- [29] Barbarossa, S., Farina, A.: 'A novel procedure for detecting and focusing moving objects with SAR based on the Wigner–Ville distribution'. IEEE Int. Radar Conf., 1990, vol. 44
- [30] Barbarossa, S.: 'Detection and imaging of moving objects with synthetic aperture radar – part 1: optimal detection and parameter estimation theory', *IEE Proc. F*, 1992, 139, pp. 79–88
- [31] Barbarossa, S., Farina, A.: 'Detection and imaging of moving objects with synthetic aperture radar – part 2: joint time-frequency analysis by Wigner–Ville distribution', *IEE Proc. F*, 1992, 139, pp. 89–97
- [32] Kirscht, M.: 'Detection and imaging of arbitrarily moving targets with single-channel SAR', *IEE Proc., Radar Sonar Navig.*, 2003, 150, pp. 7–11
- [33] Dias, J.M.B., Marques, P.A.C.: 'Multiple moving target detection and trajectory estimation using a single SAR sensor', *IEEE Trans. Aerosp. Electron. Syst.*, 2003, 39, pp. 604–624
- [34] Marques, P.A.C., Dias, J.M.B.: 'Moving targets processing in SAR spatial domain', *IEEE Trans. Aerosp. Electron. Syst.*, 2007, 43, pp. 864–874
- [35] Minardi, M.J., Gorham, L.A., Zelnio, E.G.: 'Ground moving target detection and tracking based on generalized SAR processing and change detection'. Proc. of SPIE, Algorithms for Synthetic Aperture Radar Imagery XII, Orlando, FL, USA, 14 June 2005, vol. 5808, pp. 156–165
- [36] Scarborough, S., Lemanski, C., Nichols, H., *et al.*: 'SAR change detection MTT'. Proc. of SPIE, Algorithms for Synthetic Aperture Radar Imagery XIII, Orlando, FL, USA, 17 May 2006, vol. 6237, pp. 62370V–1–62370V–11
- [37] Minardi, M.J., Zelnio, E.G.: 'Comparison of SAR based GMTI and standard GMTI in a dense target environment'. Proc. of SPIE, Algorithms for Synthetic Aperture Radar Imagery XIII, Orlando, FL, USA, 17 May 2006, vol. 6237, pp. 62370X–1–62370X–10
- [38] Holston, M.E., Minardi, M.J., Temple, M.A., *et al.*: 'Characterizing geolocation ambiguity responses in synthetic aperture radar: ground moving target indication'. Proc. of SPIE, Algorithms for Synthetic Aperture Radar Imagery XIV, Orlando, FL, USA, 7 May 2007, vol. 6568, pp. 656809–656809–11
- [39] Newstadt, G.E., Zelnio, E.G., Gorham, L., *et al.*: 'Detection/tracking of moving targets with synthetic aperture radars'. Proc. of SPIE, Algorithms for Synthetic Aperture Radar Imagery XVII, Orlando, FL, USA, 5 April 2010, vol. 7699, pp. 7699DI–1–7699DI–10
- [40] Munson, D.C.Jr., O'Brien, J.D., Jenkins, W.K.: 'A tomographic formulation of spotlight-mode synthetic aperture radar', *Proc. IEEE*, 1983, 71, (8), pp. 917–925
- [41] Webb, J.L.H., Munson, D.C.Jr.: 'SAR image reconstruction for an arbitrary radar path'. 1995 Int. Conf on Acoustics, Speech, and Signal Processing, Detroit, MI, 09 May 1995–12 May 1995, vol. 4, pp. 2285–2288
- [42] Carrara, W.G., Goodman, R.S., Majewski, R.M.: '*Spotlight synthetic aperture radar signal processing algorithms*' (Artech House, Norwood, MA, USA, 1995)
- [43] Jakowatz, C.V.Jr., Wahl, D.E., Eichel, P.H., *et al.*: '*Spotlight-mode synthetic aperture radar: a signal processing approach*' (Kluwer Academic Publishers, Norwell, MA, USA, 1996)
- [44] Xiao, S., Munson, D.C.Jr.: 'Spotlight-mode SAR imaging of a three-dimensional scene using spectral estimation techniques'. 1998 IEEE Int. Geoscience and Remote Sensing Symp. Proc., 1998. IGARSS '98, 1998, vol. 2, pp. 642–644